# **MASS SPECTROMETRY**

# 1

## **IONIZATION METHODS**

Electron ionization (EI) is surely the ionization method most widely employed (Mark and Dunn, 1985). This method was proposed and used from the early days of mass spectrometry (MS) applications in the chemical world and is still of wide interest. This interest is due to the presence of libraries of EI mass spectra, which allows easy identification of unknown previously studied analytes. The EI method suffers from two limitations: It is based on the gas-phase interactions between the neutral molecules of the analyte and an electron beam of mean energy 70 eV. This interaction leads to the deposition of internal energy in the molecules of the analyte, which is reflected in the production of odd-electron molecular ([M]<sup>++</sup>) and fragment ions. These ions are highly diagnostic from a structural point of view.

Then, the first limitation of EI is related to sample vaporization, usually obtained by heating the sample under vacuum conditions ( $10^{-5}$ –  $10^{-6}$  Torr) present in the ion source. Unfortunately, for many classes of compounds the intermolecular bonds (usually through hydrogen bridges) are stronger than the intramolecular ones and the result of heating is the pyrolysis of the analyte. The EI spectrum so obtained is not that of analyte, but that of its pyrolysis products. As examples of

this behavior one can consider saccarides, peptides, and generally all highly polar compounds.

The second limitation of EI is related to internal energy deposition. For many classes of compounds it is too high, leading to extensive fragmentation of the molecule and to the absence of a molecular ion, generally considered the most important information received from a mass spectrometric measurement.

However, EI can be, and is, successfully employed in the analysis of volatile compounds and is mainly employed linked to gas chromatographic methods (GC/MS). This approach has been extensively used in the field of grape and wine chemistry, allowing to obtain valid results on low molecular weight, low-medium polarity compounds, as described in Part II.

To overcome the second limitation described above, in the 1960s a new ionization method was proposed, based not on a physical interaction, but on gas-phase reactions of the analyte with acid or basic ions present in excess inside an ion source, and operating at a pressure in the order of  $10^{-1}$ – $10^{-2}$ Torr. This method is usually called chemical ionization (CI) (Harrison, 1983).

Generally, analyte protonation reactions are more widely employed. The occurrence of such reactions is related to the proton affinity (PA) of M and that of the reactant gas. The internal energy of the obtained species are related to the difference between these proton affinities. Thus, as an example, consider an experiment performed on an organic molecule M with a PA value of  $180\,\text{kcal/mol}$  (PA<sub>M</sub>), it can be protonated by reaction with  $CH_5^+(PA_{CH_4}=127\,\text{kcal/mol})$   $H_3O^+(PA_{H_2O}=165\,\text{kcal/mol})$ , but not with  $NH_4^+(PA_{NH_3}=205\,\text{kcal/mol})$ . This example shows an important point about CI: It can be effectively employed to select species of interest in complex matrices. In other words, by a suitable selection of a reacting ion  $[AH]^+$  one could produce  $[MH]^+$  species of molecules with a PA higher than that of A. Furthermore, the extension of fragmentation can be modified in terms of the difference of  $[PA_M-PA_A]$ .

From an operative point of view, CI is simply obtained by introducing the neutral reactant species inside an EI ion source in a "close" configuration, by which quite high reactant pressure can be obtained. If the operative conditions are properly set, the formation of the abundant [AH]<sup>+</sup> species (or, in the case of negative ions, B<sup>-</sup> species) is observed in high yield. Of course, particular attention must be paid to the case of quantitative analysis that carefully reproduces these experimental conditions, because they reflect substantially on the values of the limit of detection (LOD).

The CI, as well as EI, requires the presence of samples in the vapor phase and consequently it cannot be applied to nonvolatile analytes. Efforts have been made from the 1960s to develop ionization methods overcoming this aspect. Among them, field desorption (FD) (Beckey, 1975) and fast-atom bombardment (FAB) (Barber et al., 1982) resulted in highly effective methods and opened new applications for MS. More recently, new techniques have become available and are currently employed for nonvolatile samples: atmospheric pressure chemical ionization (APCI) (Bruins, 1991), electrospray ionization (ESI) (Yamashita and Fenn, 1984a), atmospheric pressure photoionization (APPI) (Robb et al., 2000), and matrix-assisted laser desorption—ionization (MALDI) (Karas et al., 1991) now represent the most used techniques for the analysis of high molecular weight, high-polarity samples.

Considering the wide, positive impact that these techniques had with the grape and wine chemistry in past years (as will be described in detail in Part II) we focus now on the in-depth description of these new methods, in order to give the reader a useful background for critical evaluation of results obtained with their use.

#### 1.1 ELECTROSPRAY IONIZATION

Electrospray is based on droplet production in the presence of strong electrical fields. The first electrospray experiments were performed by Jean-Antoine Nollet (physicist and Abbé), who in 1750 observed that water flowing from a small hole of an electrified metal container aerosolized when placed near the electrical ground. At that time, physics, chemistry, physiology, and medicine were very often seen as a unique science and some experiments were performed at the physiological level. Abbé Nollet observed that "a person, electrified by connection to a high-voltage generator (hopefully, well insulated from the ground!—authors' note) would not bleed normally if he was to cut himself; blood sprays from the wound" (ORNL Review, 1995).

About one century later, Lord Kelvin studied the charging between water dripping from two different liquid nozzles, which leads to electrospray phenomena at the nozzles themselves (Smith, 2000). In the last century, a series of systematic studies on electrospray were carried out by Zeleny (Zeleny, 1917) and Taylor (Taylor, 1964a and b) allowing a detailed description of the phenomenon. In the middle of the century, electrospray started to be used on the industrial scale, in the application of paints and coatings to metal surfaces. The fine spray results in very smooth even films, with the paint actually attracted to

the metal. Miniaturized versions of electrospray are even finding their way into the next generation of microsatellites: The electrostatic plume makes an efficient, although very low power, ion propulsion engine.

Electrospray became of analytical interest in 1968, when Dole and co-workers produced gas-phase, high molecular weight polystyrene ions by electrospraying a benzene–acetone solution of the polymer (Dole et al., 1968). Quite strangely, these results did not lead to further applications until 1984, when the studies of Yamashita and Fenn (Yamashita and Fenn, 1984b) brought electrospray to the analytical world and from which electrospray applications have grown fantastically.

This technique can be considered the ionization method that the entire scientific community was waiting for. This method is an effective and valid approach for the direct study of analytes present in solution, without the need of analyte vaporization and, consequently, for an easy coupling with LC methods. Furthermore, in the same time period methods able to give information on large biomolecules was growing. In this framework, the behavior in electrospray conditions of proteins and peptides (as well as oligonucleotides), reflecting on the production of multiply charged ions, makes this ionization method essential in biomedical studies and in proteome investigations. For this last reason, the Nobel Price in 2002 was assigned to Fenn, with the official sentence "for the development of soft desorption ionization methods for mass spectrometric analyses of biological macromolecules".

This chapter aims to offer a concise description of chemical-physical phenomena that are at the base of the ESI.

### **1.1.1** The Taylor Cone

The instrumental setup for ESI experiments is schematized in Fig. 1.1. The solution is injected into a stainless steel capillary (10<sup>-4</sup> m o.d.). A voltage on the order of kilovolts is applied between this capillary and a counterelectrode, which is placed a few-tenths of a millimeter away from it. In general, as the liquid begins to exit from the needle, it charges up and assumes a conical shape, referred to as the Taylor cone, in honor of Taylor who first described the phenomenon in 1964. The liquid assumes this shape because when charged up, a conic shape can hold more charge than a sphere. The formation of this cone-shaped structure can be justified by the presence of charged species inside the solution that experiment with the effect of the electrostatic field existing between the capillary and the counterelectrode. What is the origin of this charged species, in the absence of ionic solute? It emphasises that even in the absence of ionic analytes, protic solvents produce ionic

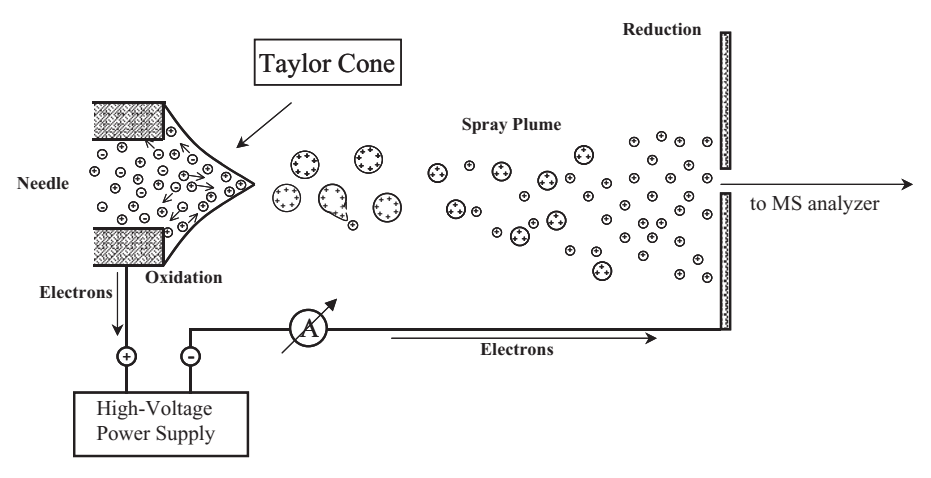


**Figure 1.1.** Schematic of an electrospray source showing the production of charged droplets from the Taylor cone.

species, due to their dissociation. Thus, for example, taking into account  $K_{\rm w}$  at 20 °C is  $10^{-14.16}$ , the  ${\rm H_3O^+}$  concentration at 20 °C is in the order of  $8.3 \times 10^{-8} \, {\rm M}$ . Analogously,  $K_{\rm a}({\rm CH_3OH}) = 10^{-15.5}$ . Consequently, the solvents usually employed for electrospray experiments already produce ions in solution, which can be considered responsible for the cone formation. Of course, the presence of dopant analytes (e.g., acids), as well as traces of inorganic salts, strongly enhance this phenomenon.

If the applied electrical field is high enough, the formation of charged droplets from the cone apex is observed which, due to their charge, further migrate through the atmosphere to the counterelectrode. Experimental data have shown that the droplet formation is strongly influenced by

- Solvent chemical–physical characteristics (viscosity, surface tension,  $pK_a$ ).
- Concentration and chemical nature of ionic analytes.
- Concentration and chemical nature of inorganic salts.
- · Voltage applied between capillary and counterelectrode.

In the case of positive-ion analysis, the capillary is usually placed at a positive voltage while the counterelectrode is placed at a negative voltage (this is the case shown in Fig. 1.1). The reverse is used in the case of negative-ion analysis. In both cases, a high number of positive (or negative) charges are present on the droplet surface.

The formation of the Taylor cone and the subsequent charged droplet generation can be enhanced by the use of a coaxial nitrogen gas stream. This instrumental setup is usually employed in the commercially available electrospray sources: Then the formation of charged droplets is due to either electrical and pneumatic forces.

Blades et al. (Blades et al., 1991) showed that the electrospray mechanism consists of the early separation of positive from negative electrolyte ions present in solution. This phenomenon requires a charge balance with conversion of ions to electrons occurring at the metal-liquid interface of the ESI capillary, in the case of positive-ion analysis. The processes that lead to a deep change of composition of ions in the spray solution are those occurring at the metal-liquid capillary interface and the related oxidation reactions were studied by the use of a Zn capillary tip. This experiment was carried out by using three different capillary structures. The passivated stainless steel capillary normally employed was substituted with one where the tip was made by Zn having a very low reaction potential  $(Zn_{(s)} \rightarrow Zn^{2+} + 2e,$  $E_{\rm red}^0 = -0.76 \,\rm V$ ). Actually, under these conditions abundant Zn<sup>2+</sup> ions were detected in the mass spectrum simply by spraying methanol (CH<sub>3</sub>OH) at a flow rate of 20µL/min. This result suggests that the oxidation reaction took place at the zinc-liquid capillary interface. In order to be confident of this hypothesis, and to exclude other possible origins of Zn<sup>2+</sup> production, a further experiment was carried out. This experiment consisted of placing a Zn capillary before the electrospray capillary line and keeping it electrically insulated. In this case, Zn<sup>2+</sup> ions were not detected. These results provide qualitative and quantitative evidence that in the case of positive-ion instrumental setup (Fig. 1.1), electrochemical oxidation takes place at the liquid-metal interface of the electrospray capillary tip.

Now, ESI can be considered as an electrolysis cell and the ion transport takes place in the liquid, not the gas phase. The oxidation reaction yield depends on the electrical potential applied to the capillary, as well as on the electrochemical oxidation potentials from the different possible reactions. Kinetic factors can exhibit only minor effects, considering the low current involved.

The effect of oxidation reactions at the capillary tip will be the production of an excess of positive ions, together with the production of an electron current flowing through the metal (see Fig. 1.1). An excess of positive ions could be the result of two different phenomena; that is, the production of positive ions themselves or the removal of negative ions from the solution.

In the case of a negative-ion source setup (spray capillary placed at negative voltage), reduction reactions usually take place with the formation of deprotonated species.

The electrical current due to the droplets motion can be measured easily by the amperometer (A) shown in Fig. 1.1. This measurement allows to estimate, from a quantitative point of view, the total number of elementary charges leaving the capillary and which, theoretically, may correspond to gas-phase ions. The droplet current I, the droplet radii R, and charge q were originally calculated by Pfeifer and Hendricks (Pfeifer and Hendricks, 1968):

$$I = \left[ \left( \frac{4\pi}{\varepsilon} \right)^3 (9\gamma)^2 \varepsilon_0^5 \right]^{1/7} (KE)^{3/7} (V_f)^{4/7}$$
(1.1)

$$R = \left(\frac{3\varepsilon\gamma^{1/2}V_f}{4\pi\varepsilon_0^{1/2}KE}\right)^{2/7} \tag{1.2}$$

$$q = 0.5 \left[ 8 \left( \varepsilon_0 \gamma R^3 \right)^{1/2} \right] \tag{1.3}$$

where  $\gamma$  is the surface tension of the solvent; K is the conductivity of the infused solution; E is the electrical field;  $\varepsilon$  is the dielectric constant of the solvent;  $\varepsilon_0$  is the dielectric constant of the vacuum; and  $V_f$  is the flow rate.

De La Mora and Locertales (De La Mora and Locertales, 1994) found, based on both theoretical calculation and experimental data, the following equations for the same quantities:

$$I = f\left(\frac{\varepsilon}{\varepsilon_0}\right) \left(\gamma K V_f \frac{\varepsilon}{\varepsilon_0}\right)^{1/2} \tag{1.4}$$

$$R \approx \left(\frac{V_f \varepsilon}{K}\right)^{1/3} \tag{1.5}$$

$$q = 0.7 \left[ 8\pi \left( \varepsilon_0 \gamma R^3 \right)^{1/2} \right] \tag{1.6}$$

where  $f(\varepsilon/\varepsilon_0)$  is a function of the  $\varepsilon/\varepsilon_0$  ratio.

Equations 1.1 and 1.4 at first seem to be strongly different, but they indicate an analogous dependence of I from the two most relevant experimental parameters (i.e., the flow rate and the conductivity).

Equations 1.2 and 1.5 both show a decrease of the droplets dimension by increasing the solution conductivity. These relationships are particularly relevant because in solution, when different electrolytes are present, the conductivity K may be obtained as the sum of the conductivities due to the different species and is proportional to the ion concentration:

$$K = \sum_{i} \lambda_{0,m,i} C_i \tag{1.7}$$

where  $\lambda_{0,m,i}$  is the molar conductivity of the electrolyte *i*.

The charged droplets, generated by solution spraying, decrease their radius due to solvent evaporation, but their total charge amount remains constant. The first step is to determine the energy required for solvent evaporation that is due to environmental thermal energy. In a second step, this process is enhanced through further heating obtained by the use of a heated capillary or by collisions with heated gas molecules. The maintenance of the total charge during this evaporation phase can be explained because the ion emission from the solution to the gas phase is an endothermic process.

The decrease of the droplet radius can be described by Eq. 1.8, where  $\overline{\nu}$  is the average thermal speed of solvent molecules in the vapor phase:

$$\frac{dR}{dt} = -\frac{\alpha \overline{\nu}}{4\rho} \frac{p^0 M}{R_g T} \tag{1.8}$$

where  $p^0$  is the solvent vapor pressure at the droplet temperature, M is the solvent molecular weight;  $\rho$  is the solvent density;  $R_g$  is the gas constant; T is the droplet temperature; and  $\alpha$  is the solvent condensation coefficient.

This relationship showed all factors that can influence the droplet dimensions, and consequently the effectiveness of ESI.

The decrease of the droplet radius with respect to time leads to an increase of surface charge density. When the radius reaches the Rayleigh stability limit (given by Eq. 1.9) the electrostatic repulsion is identical to the attraction because of surface tension. For lower radii, the charged droplet is unstable and decomposes through a process generally defined as Columbic fission (Rayleigh, 1882). This fission is not regular (i.e., the two parts originated by it do not necessarily have analogous dimensions).

$$q_{R_{y}} = 8\pi \left(\varepsilon_{0} \gamma R^{3}\right)^{1/2} \tag{1.9}$$

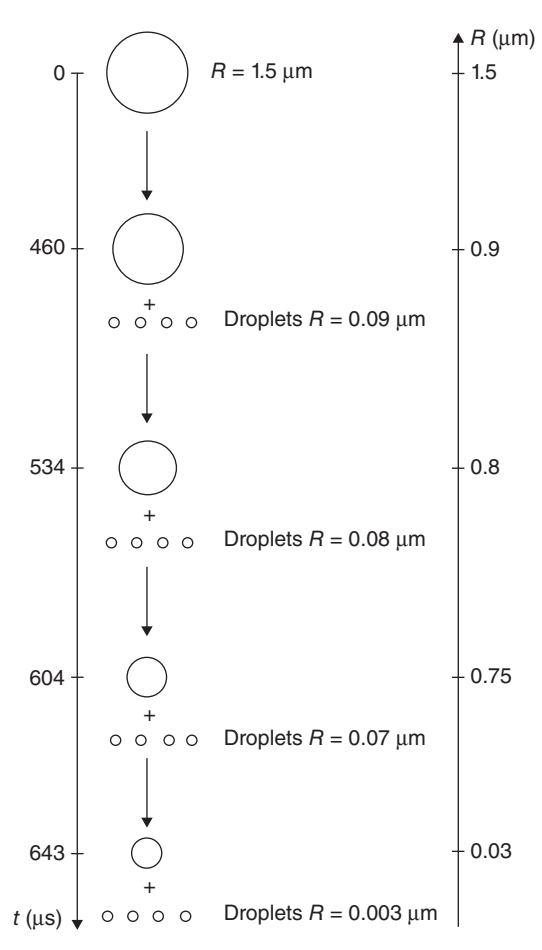
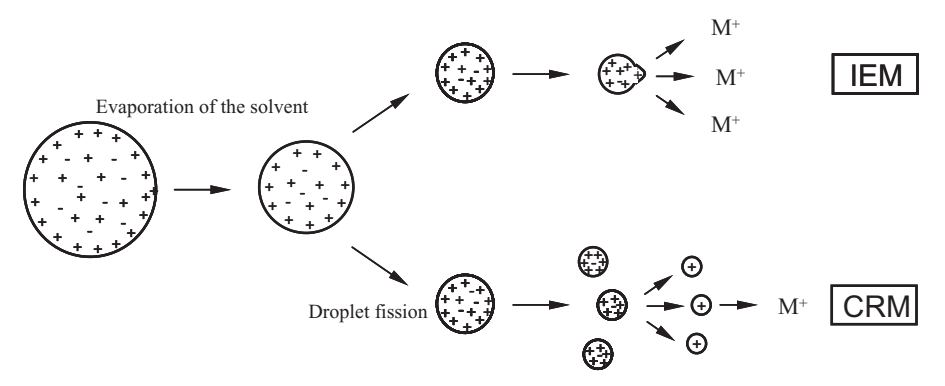


Figure 1.2. Data obtained by theoretical calculation of drop dimensions and lifetime.

Detailed studies performed by Gomez and Tang (Gomez and Tang, 1994) allowed to calculate the lifetime and the fragmentation of droplets. An example is shown in Fig. 1.2.

Until now two different mechanisms have been proposed to give a rationale for the formation of ions from small charged droplets. The first recently was discussed by Cole (Cole, 2000) and Kebarle and Peschke (Kebarle and Peschke, 2000). It describes the process as a series of scissions that lead at the end to the production of small droplets having one or more charges, but only one analyte molecule. When the last few solvent molecules evaporate, the charges are localized on the analyte substructure, which give rise to the most stable gas-phase ion. This model is usually called the charged residue mechanism (CRM) (see lower part of Fig. 1.3).



**Figure 1.3.** Mechanisms proposed for the formation of ions from small charged droplets: ion evaporation mechanism (IEM) and charge residue mechanism (CRM).

Thomson and Iribarne (Thomson and Iribarne, 1979) proposed a different mechanism, in which a direct emission of ions from the droplet is considered. It occurs only after the droplets have reached a critical radius. This process is called ionic evaporation mechanism (IEM) and is dominant with respect to Columbic fission from particles with radii  $r < 10\,\mathrm{nm}$  (see upper part of Fig. 1.3).

Both CRM and IEM are able to explain many of the behaviors observed in ESI experiments. However, a clear distinction between the two mechanisms lies in the way by which an analyte molecule is separated from the other molecules (either of analyte or solvent present in droplets). In the case of IEM, this separation takes place when a single-analyte molecule, bringing a part of the charge in excess of the droplet, is desorbed in the gas phase, thus reducing the Columbic repulsion of the droplets. In the CRM mechanism, this separation occurs through successive scissions, reducing the droplet dimensions until only one single molecule of analyte is present in them. In general, the CRM model remains valid in the process of gas-phase ion formation for high molecular weight molecules.

#### 1.1.2 Some Further Considerations

What was just described can give us an idea of the high complexity of the ESI process: The ion formation depends on many different mechanisms occurring either in solution or during the charged droplets production and ion generation from the droplets themselves.

First, the ESI users must consider that the concentration of the analyte present in the original solution does not correspond to that present in the droplets generating the gas-phase ions. This point must be carefully considered when the original solution is far from neutrality. In this case, the pH will show sensible changes. Gatling and Turecek (Gatling and Turecek, 1994) studying the  $Fe^{2+}(bpy)_3$   $Ni^{2+}(bpy)_3$  (bpy = 2,2'-bipyridine) complex dissociation under electrospray conditions, found that an apparent increase of  $[H_3O^+]$  in the order of  $10^3-10^4$ -fold with respect to the bulk solution is observed. Furthermore, due to solvent evaporation, the pH value is not homogeneous inside the droplet. A spherical microdroplet is estimated to maintain a pH 2.6–3.3 in a 5–27-nm thick surface layer without exceeding the Rayleigh limit. This limit implies that complex dissociations occur near the droplet surface of high-local acidity.

For polar compounds, the surface charge density present in the droplet can activate some decomposition reaction of the analyte. In the study of  $[Pt(\eta^3\text{-allyl})XP(C_6H_5)_3]$  complexes (X=Cl or Br), the formation of any molecular species in the ESI condition was not observed (Favaro et al., 1997). This result is quite surprising, considering that the same compounds lead to molecular species either in fast-atom bombardment (FAB) or under electron ionization conditions (i.e., in experimental conditions surely "harder" than ESI). This result has been linked to the occurrence of phenomena strictly related to the ESI condition and explained by the high positive charge density present on the droplet surface. It can activate the formation, in the polar molecule under study, of an ion pair consisting of  $X^-$  and  $[M-X]^+$  (X=Cl or Br) (see Fig. 1.4). The latter are the only species detectable in positive-ion ESI conditions.

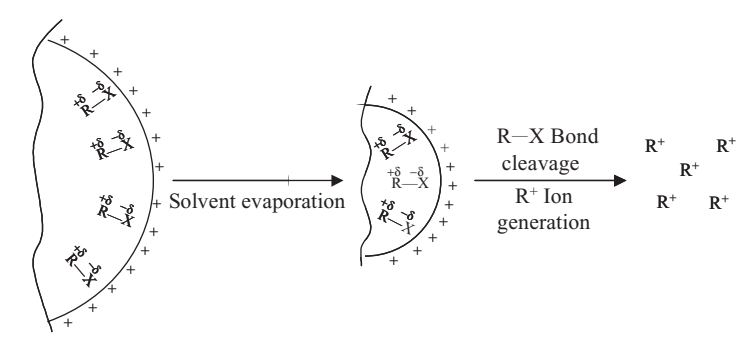


**Figure 1.4.** Formation of  $R^+$  species ( $[Pt(\eta^3-allyl)P(C_6H_5)_3]^+$ ) from  $[Pt(\eta^3-allyl)XP(C_6H_5)_3]$  complexes, due to the formation of an ion pair catalyzed by the high surface charge density present in the droplet.

#### 1.1.3 Positive- and Negative-Ion Modes

As described in Section 1.1.2, the ESI source can lead to the production of positive or negative ions, depending on the potentials applied to the sprayer and the related counterelectrode. Some producers follow the original ESI source design, placing the sprayer at some kilovolts (positive for positive-ion analysis, negative for negative-ion production) and the counterelectrode (i.e., the entrance to the mass analyzer) grounded or at a few volts (see the left-hand side of Fig. 1.5 for positive-ion analysis). Some other producers use a different potential profile, placing the sprayer at ground potential and the counterelectrode at + or – kilovolts for production of negative or positive ions respectively (right-hand side of Fig. 1.5).

In ESI conditions, aside from the formation of protonated ( $[M + H]^+$ ) and deprotonated ( $[M - H]^-$ ) molecules arising from the oxidation–reduction reactions at the sprayer, some cationization and anionization reactions can take place, due to the presence, inside the solution, of cations and anions. As an example, the positive- and negative-ion spectra of secoisolariciresinol diglucoside (SDG), obtained by injecting the methanol solution ( $10^{-5}M$  with 0.1% of formic acid) in the ESI source at a flow rate of  $15\mu L/min$ , are reported in Fig. 1.6a and b, respectively. In the former case, the protonated molecule is detectable at m/z 687, but the most abundant peaks are present at m/z 704 and 709, due to cationization reactions with  $NH_+^4$  and  $Na_+^4$ , respectively. A scarcely abundant adduct with  $K_-^4$  is also detectable at m/z 725. The negative-ion spectrum (Fig. 1.6b) shows an abundant peak due to a deprotonated molecule (m/z 685), together with those due to adducts with  $Cl_-^4$  and  $HCOO_-^4$  (m/z 721 and 731, respectively).

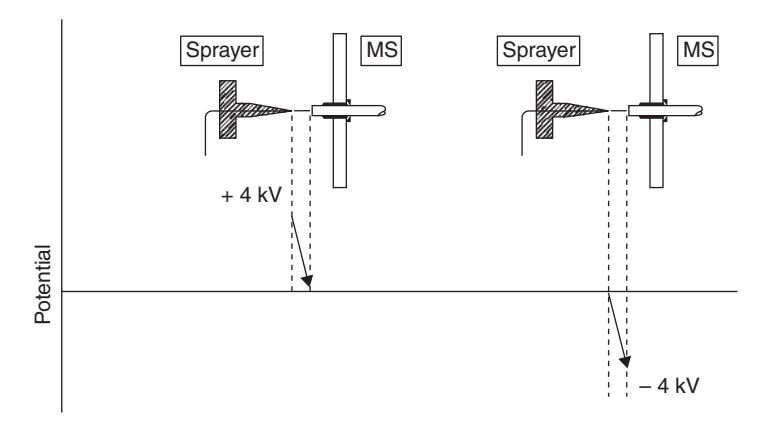
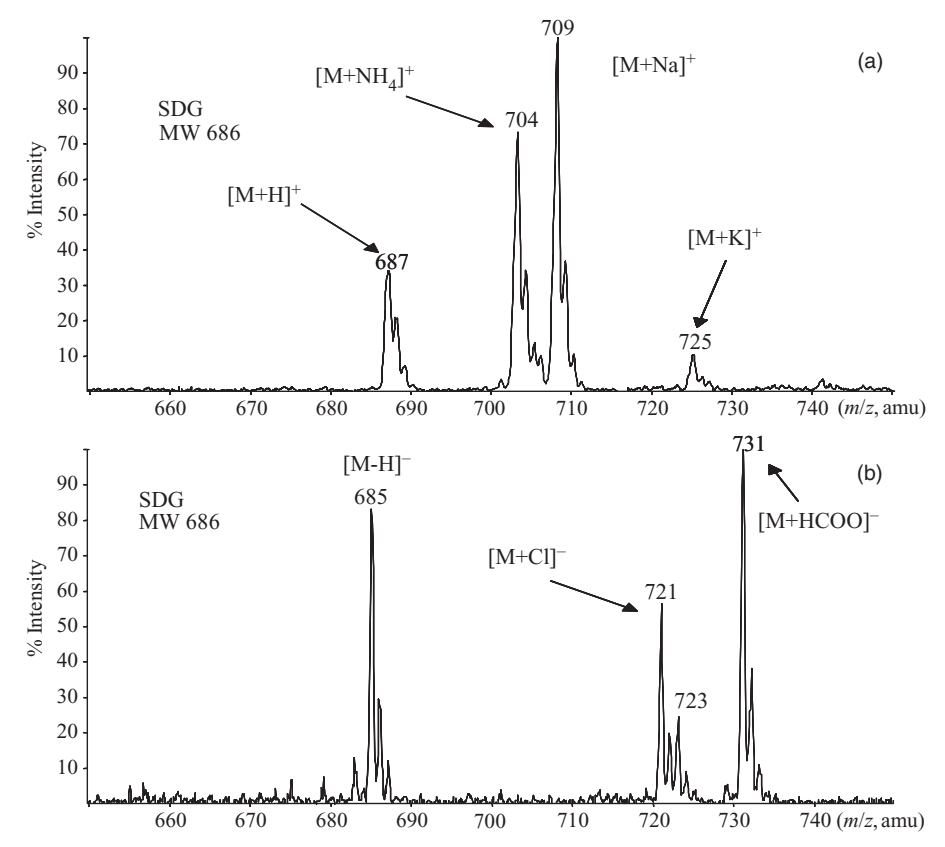


Figure 1.5. Potential profiles usually employed in ESI/MS for positive-ion analysis.



**Figure 1.6.** The ESI spectra of SDG showing the presence of a wide number of adducts: (a) positive and (b) negative ions.

The privileged formation of molecular species makes the ESI method highly interesting for the analysis of complex mixtures, without the need of previous chromatographic separation. By direct infusion of the mixture dissolved in a suitable solvent, it is possible to obtain a map of the molecular species present in the mixture itself. Furthermore, by operating in the positive-ion mode it is possible to see the compounds with the highest proton affinity values (i.e., the most basic ones), while in the negative-ion mode the formation of ions from the most acidic species will be privileged .

This aspect is well described by the ESI spectra reported in Fig. 1.7, which is obtained by direct infusion of a CH<sub>3</sub>OH/H<sub>2</sub>O (1:1) solution of an extract of Cynara scolymus. The positive-ion spectrum (Fig. 1.7a) is highly complex either for the complexity of the mixture under analysis, or for the possible ionization of the various molecular species by

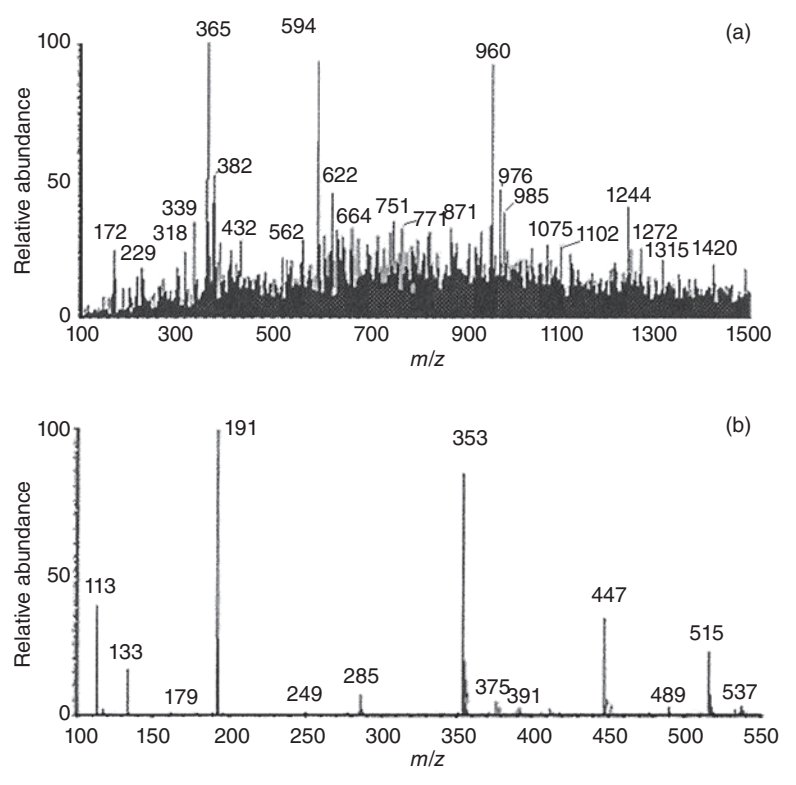


**Figure 1.7.** Positive (a) and negative (b) ion ESI spectra of an extract of Cynara scolymus, obtained by direct infusion of its (CH<sub>3</sub>OH/H<sub>2</sub>O, 1:1) solution.

addition of H<sup>+</sup>, Na<sup>+</sup>, K<sup>+</sup>, and NH<sub>4</sub><sup>+</sup>. On the contrary, the negative-ion spectrum (Fig. 1.7b) is due to few, well-defined ionic species. The chemical background observed in positive-ion mode is completely suppressed. The two most abundant ions at m/z 191 and 353 correspond, as proved by MS-MS experiments, to molecular anion species ([M-H]-) of isoquercitrin and chlorogenic acid, respectively. In the higher m/zregion, the ion at m/z 515 originates from cinarin. Ions at m/z 447 and 285, detected in low abundance, correspond to luteolin-7-O-glucoside and luteolin, respectively. It is interesting to observe that these species are completely undetectable in the positive-ion ESI spectrum (Fig. 1.7a), being completely lost in the chemical background. This result can be explained by the chemical nature of these compounds. The carboxylic and phenolic hydroxyl groups present in them are easily deprotonated to give the corresponding molecular anion species, whereas they do not easily undergo protonation to give the corresponding molecular cation species, which are thermodynamically unfavorable.

#### 1.1.4 Micro- and Nano-LC/ESI/MS

Electrospray is surely the ionization method most widely employed for the liquid chromatography (LC)-MS coupling (Cappiello, 2007). The possibility of performing ionization at atmospheric pressure [also obtained in the case of atmospheric pressure chemical ionization (APCI) and atmospheric pressure photoionization (APPI), allows the direct analysis of analyte solutions. However, some problems arise from the intrinsically different operative conditions of the two analytical methods. First, there are the high-vacuum conditions that must be present at the mass analyzer level. Second, the mass spectrometers generally exhibit a low tolerance for the nonvolatile mobile-phase components, usually employed in LC conditions to achieve high chromatographic resolution.

Summarizing, the difficulties in LC/MS coupling can be related to the following aspects:

- Sample restriction: The differences among different classes of samples in terms of molecular weight, polarity, and stability (either from the chemical or the chemical–physical point of view) requires an accurate setup of the ESI source conditions;
- Solvent restriction: The LC mobile phase is generally a solvent mixture of variable composition. This variability necessarily reflect on the formation in ESI conditions of droplets of different dimension and lifetime (i.e., under somewhat different ionization conditions). Also in this case an indepth evaluation of the ESI source parameters must be performed to achieve results as close as possible.
- Chromatographic eluate flow, which must be compatible with the sprayer operative flow.

The scheme of a LC/ESI/MS system is shown in Fig. 1.8. Depending of the LC solvent flow, the splitter S can be employed to reduce the

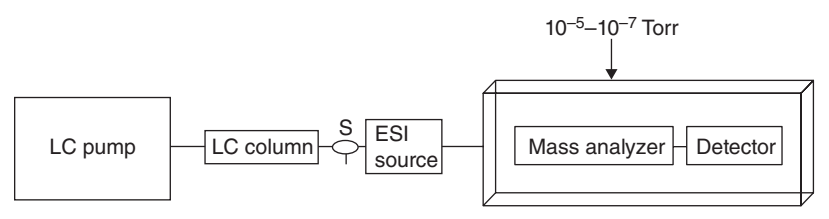


**Figure 1.8.** Scheme of the LC/ESI/MS system.

flow itself to values suitable for the ESI sprayer. Of course, the split ratio reflects on a decrease of sensitivity (a portion of the sample is dropped away). Analytical columns with internal diameters (i.d.) in the range 2.1–4.6 mm require the use of the splitter, while columns with i.d. ≤1 mm can be directly connected with the ESI source.

Note that, aside from the splitting problem, the i.d. reduction of LC columns leads to a sensible increase in sensitivity of the LC/ESI/MS system. In fact, as shown schematically in Fig. 1.9, the i.d. reduction leads to a higher analyte concentration, due to the volume reduction: Then, passing from a 4.6 to a 1.5 mm i.d. column, a decreased volume of one order of magnitude is obtained. This result reflects in a 10 times increase of analyte concentration and the consequent increase of the MS signal.

This aspect has led to the production of micro- and nanoelectrospray sources, where the chromatographic eluate flow is in the range  $1-10^{-2}\mu L/min$ . A typical instrument setup for nano-ESI experiments is shown in Fig. 1.10. In this case, the supplementary gas flow for spray generation is no longer present and the spray formation is only due to the action of the electrical field. The sprayer capillary, with an internal

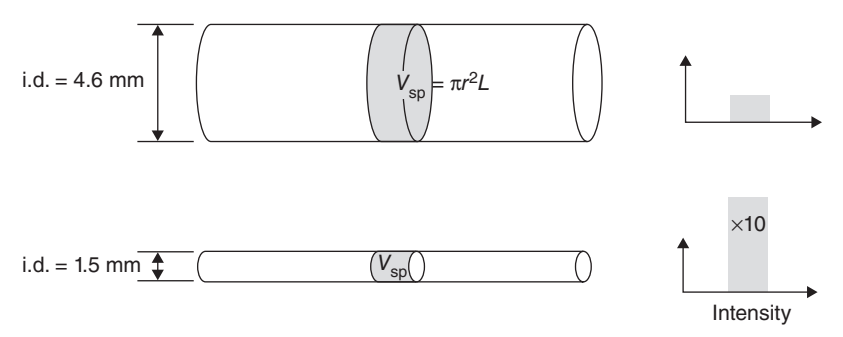


**Figure 1.9.** Comparison of the behavior of two LC columns of different internal diameter, operating with the same linear velocity. In the case of a low i.d. column, a higher analyte concentration is present, reflecting in a higher signal intensity.

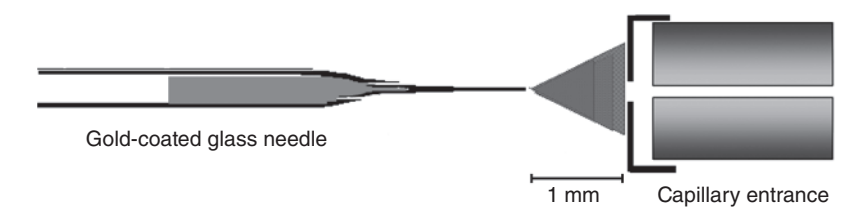


Figure 1.10. Typical instrumental configuration for nano-ESI experiments.

diameter in the range 5– $20\,\mu m$ , is coated with a conductive film (e.g., gold film) in order to be placed at the correct electrical potential.

Just to give an idea of the nano-ESI performances, when the electrical field is applied, a spray is generated with a flow rate in the order of  $25-100\,\text{nL/min}$ . This finding means that  $1\,\mu\text{L}$  of sample can be sprayed for ~40 min! This result reflects in a system with high sensitivity and requires a very low sample quantity.

The main reason for moving to low-flow LC/MS systems is to handle the analytes in the smallest possible volume. Thus, by using an enrichment column, the sample can be trapped and then eluted in the smallest possible volume, so as to reach maximum concentration levels. This approach has required the development of a nanopump. The related technology is nowadays available on the market, but the weak point of the nanopump—nanocolumn—nano-ESI system is mainly related to the connections among the three components, introducing dead volumes and the possibility of small, undetectable leaks.

Recently, a new approach was proposed to overcome these problems, based on a microfluidic chip device (Agilent, 2007) (Fig. 1.11). This finding includes the enrichment column, the separation column, and the nanospray emitter. By use of a robotic system, the chip is automatically positioned in front of the entrance orifice of the mass spectrometer.

The full LC-chip/MS system includes an autosampler and capillary LC pump for delivery of the sample to the enrichment column, which allows sample loading of larger volume samples in a short period of

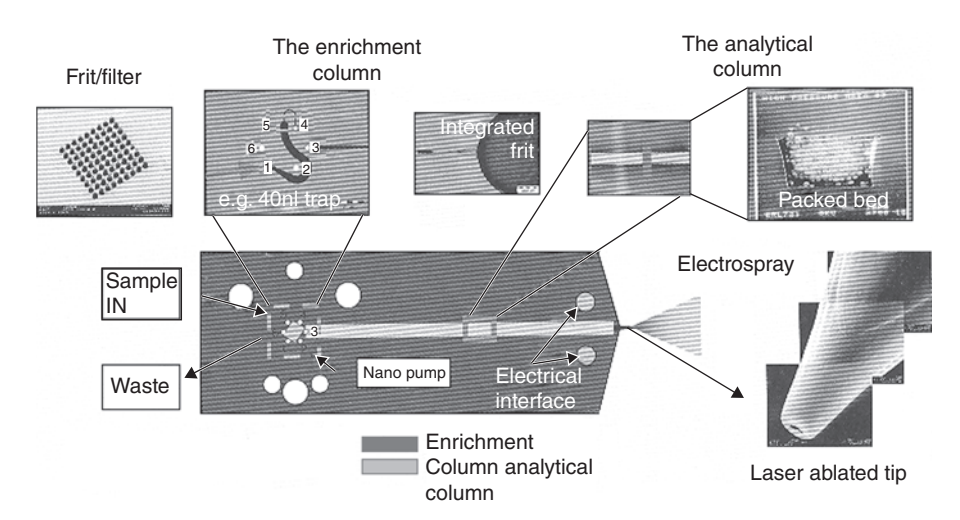


Figure 1.11. Scheme of the full LC-chip-MS system. (Agilent, technical literature).

time, by using a higher loading flow rate (e.g.,  $4\mu L/min$ ). The analytical column is driven by a nano-LC pump typically operating at  $100-600\,nL/min$ .

#### 1.2 ATMOSPHERIC PRESSURE CHEMICAL IONIZATION

As described in the introduction, CI was developed in the 1960s as an alternative ionization method to EI being able to induce a low-energy deposition in the molecule of interest, reflecting on the privileged formation of charged molecular species (Harrison, 1983). Chemical ionization is based on the production in the gas phase, at a pressure in the range  $10^{-1}$ –1Torr, of acidic or basic species, which further react with a neutral molecule of analyte leading to  $[M + H]^+$  or  $[M - H]^-$  ions, respectively.

Atmospheric pressure chemical ionization (Bruins, 1991) was developed starting from the assumption that the yield of a gas-phase reaction depends not only on the partial pressure of the two reactants, but also on the total pressure of the reaction environment. For this reason, the passage from the operative pressure of 0.1–1 Torr, present inside a classical CI source, to atmospheric pressure would, in principle, lead to a relevant increase in ion production, which consequently leads to a relevant sensitivity increase. Furthermore, the presence of air at atmospheric pressure can play a positive role in promoting ionization processes.

At the beginning of research devoted to the development of an APCI method, the problem was the choice of an ionizing device. The most suitable and effective one was, and still is, a corona discharge. The importance of this ionization method lies in its possible application to the analysis of compounds of interest dissolved in suitable solvents: The solution is injected into a heated capillary (typical temperatures in the range 350–400 °C), which behaves as a vaporizer. The solution is vaporized and reaches, outside from the capillary, the atmospheric pressure region where the corona discharge takes place. Usually, vaporization is assisted by a nitrogen flow coaxial to the capillary (Figs. 1.12 and 1.13). The ionization mechanisms are typically the same as those present in CI experiments.

The needle generates a discharge current of ~2–3  $\mu$ A, which ionizes air producing primary ions (mainly N<sub>2</sub><sup>+</sup>, O<sub>2</sub><sup>+</sup>, H<sub>2</sub>O<sup>+</sup>, and NO<sup>+</sup> in the positive mode, O<sub>2</sub><sup>-</sup>, O<sup>-</sup>, NO<sub>2</sub><sup>-</sup>, NO<sub>3</sub><sup>-</sup>, O<sub>3</sub><sup>-</sup>, and CO<sub>3</sub><sup>-</sup> in the negative mode). Primary ions react very rapidly (within 10<sup>-6</sup>s) transferring their charge to solvent molecules, in a reaction controlled by the

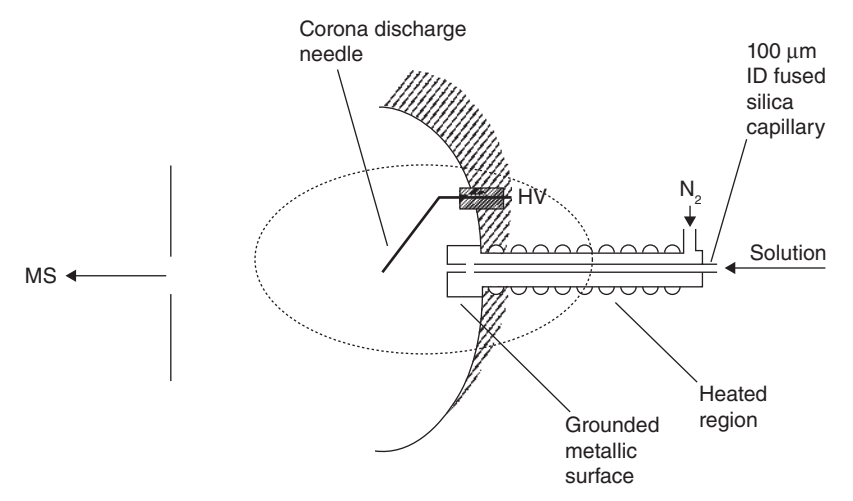


**Figure 1.12.** Scheme of the APCI ion source.

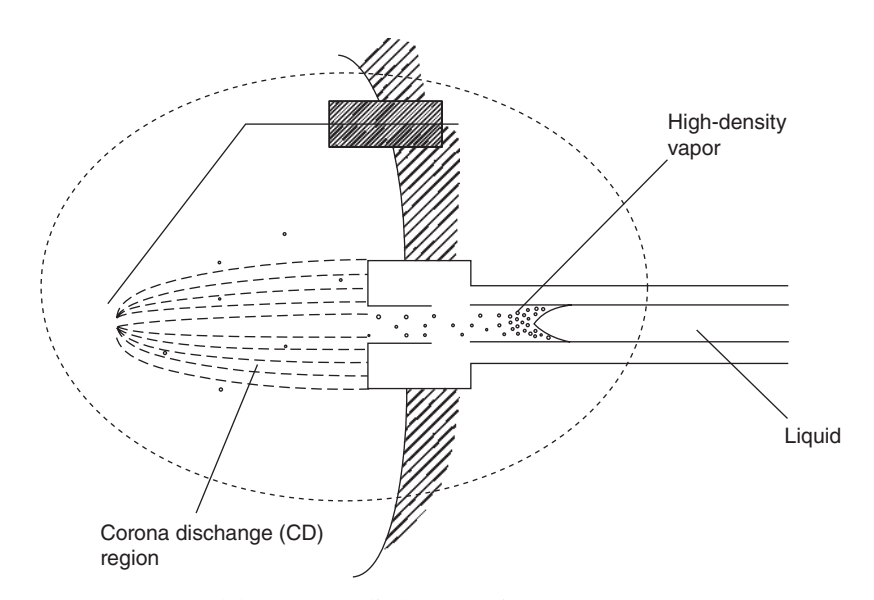


Figure 1.13. Corona discharge region of an APCI source.

recombination energy of the primary ions themselves, to produce the effective CI reactant ions. These are characterized by a longer lifetime ( $\sim 0.5 \times 10^{-3}$  s) and react with analyte molecules to produce analyte quasimolecular ions by charge- or proton-transfer reactions, according to the proton affinity of the analyte itself. The total reaction time in the source corresponds in practice to the final proton transfer ( $\sim 0.5 \times 10^{-3}$  s) as the time of the preceding solvent ionization can be

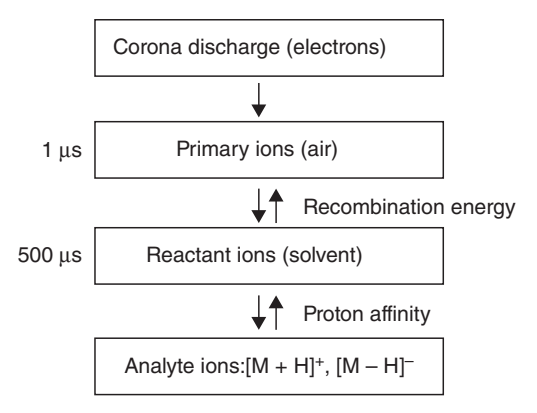


Figure 1.14. Sequence and time scale of the reactions occurring in an APCI ion source.

disregarded. The whole ionization cascade is represented in Fig. 1.14. Under these conditions, the formation of protonated ( $[M + H]^+$ ) or deprotonated ( $[M - H]^-$ ) molecules is generally observed operating in the positive- or negative-ion mode, respectively.

One problem that APCI exhibited at the beginning of its development was the presence of still solvated analyte molecules (i.e., the presence of clusters of analyte molecules with different numbers of solvent molecules). To obtain a declustering of these species, different approaches have been proposed, among which nonreactive collision with target gases (usually nitrogen) and thermal treatments, are those considered to be most effective and currently employed. Different instrumental configurations, based on a different angle between the vaporizer and entrance capillary (or skimmer) have been proposed;  $180^{\circ}$  (in line) and  $90^{\circ}$  (orthogonal) geometries are those most widely employed.

#### 1.3 ATMOSPHERIC PRESSURE PHOTOIONIZATION

Photoionization has been considered, from the beginning of analytical MS, to be highly attractive; it exhibits some theoretical advantages with respect to electron ionization, but also has some severe limitations (Morrison, 1986).

In general, the energy transfer involved in ionization of atoms and molecules must be enough to excite one electron from a bond to an unquantized orbital. The ionization energy is just the lowest energy value required for the occurrence of this phenomenon.

For electron ionization, this process can be written as:

$$M + e^- \rightarrow [M^*]^- \rightarrow M^{+\bullet} + 2e^-$$

where three events occur, according to Wigner (Wigner, 1968): (1) approach of an electron to a neutral molecule, (2) formation of a collisional complex, (3) dissociation of the complex in a positive ion and two electrons. The probability of ionization is critically dependent on step (3). Wannier (Wannier, 1953) has shown that this probability depends on the number of freedom degrees n for sharing the excess energy between the electrons. By defining  $E_c$  the minimum energy, the ionization probability can be defined as:

$$P(E-E_c) = k(E-E_c)^n$$
 (1.10)

and, in the case of emission of two electrons from the collision complex, n = 1.

For photoionization, the basic reaction becomes

$$M + h v \rightarrow [M^*] \rightarrow M^{+\bullet} + e^-$$

and, by using the Wigner and Wannier arguments, in this case the probability expressed by Eq. 1.10 will have n < 1 of the value for the EI-induced process. This finding implies that the ionization probability as a function of photon energy will be zero until the ionization energy is reached. When the ionization energy (IE) is reached, the probability will rise immediately to the value determined by the electronic transition probability for the process. In other words, the necessary condition to obtain the photoionization of a molecule M is that  $IE_M \le hv$  (i.e., that the ionization energy of M is lower than the photon energy).

The main limitation to the extensive use of photoionization in MS was that at the light frequencies suitable to produce ionization of most organic compounds (IE ranging up to 13 eV) it is not possible to use optical windows in the path of the light beam. All the window materials are essentially opaque at this photon energy. Consequently, the light source, usually involving a gas discharge, must be mounted inside the ion source housing operating under high-vacuum conditions. A further aspect that in the past limited the common use of photoionization was surely the low sensitivity of the method. When operating under high-vacuum conditions, typical of classical ion sources, the formation of ions is some orders of magnitude lower than is observed with the same sample density in EI conditions. This finding can be related to the photon cross section.

However, note that photoionization has been used since 1976 as a detection method in GC, proving that, when the sample density is high enough, good sensitivity can be achieved, together with the specificity related to the wavelength employed.

Only a few papers appeared in the past on analytical applications of photoionization in MS. Among them, that by Chen et al. showed the analytical power of the method (Chen et al., 1983) by employing an argon resonance lamp emitting photons with energies of 11.6 and 11.8 eV with an intensity of  $3 \times 10^{12}$  photons s<sup>-1</sup>. The interaction of a mixture of alkanes in nitrogen (at a pressure of  $10^{-2}$ Torr) with the light beam led to good quality mass spectra, with a detection limit of ~10 ppb. Analogous results were achieved by Revel'skii et al. (Revel'skii et al., 1985).

Of course, with high-power lasers, the photoionization is no longer limited to photons whose energy exceeds that of the ionization energy, since multiphoton processes now become operative. However, the use of a "conventional" light beam interacting with high-density vapors coming from the vaporization of the sample solution has been considered of interest and the Bruins' group (Robb et al., 2000) developed and tested the first experimental apparatus, devoted to LC/MS experiments. By considering the analogies with the well-established APCI technique, this new method was called APPI.

In an APPI source, a series of different processes can be activated by photon irradiation. Calling ABC the analyte molecule, S the solvent, and G other gaseous species present in the source  $(N_2, O_2, \text{ and } H_2O \text{ at trace level})$ , the first step can be considered their photoexcitation:

$$ABC + hv \rightarrow ABC^*$$
  
 $S + hv \rightarrow S^*$   
 $G + hv \rightarrow G^*$ 

At this stage, inside the source, a collection of excited and nonexcited species is present and a series of further processes can occur, as:

$$ABC^* \rightarrow ABC + hv$$
 Radiative decay  
 $ABC^* \rightarrow AB^* + B^*$  Photodissociation  
 $ABC^* \rightarrow ACB^*$  Isomerization  
 $ABC^* + S \rightarrow ABC + S^*$   
 $ABC^* + G \rightarrow ABC + G^*$  Collisional quenchin  
 $ABC + S^* \rightarrow ABC^* + S$ 

Only when  $hv \ge IE$ , can ionization take place

$$ABC^* \rightarrow ABC^{+\bullet} + e^{-}$$

$$S^* \rightarrow S^{+\bullet} + e^{-}$$

$$G^* \rightarrow G^{+\bullet} + e^{-}$$

Recombination processes can occur as well. Hence, inside an ion source at atmospheric pressure, a highly complex mixture of ions, neutrals at ground and excited states, radicals and electrons, is photogenerated.

To put some order in this complex environment, the photon energy can be chosen in order to avoid the ionization processes of the S and G species.

The plot of intensity versus frequency of the most commonly employed lamps is reported in Fig. 1.15. By these data, it can be deducted that the Kr lamp is most suitable for analytical purposes. It shows an energy distribution from 8 to  $10\,\mathrm{eV}$ , and consequently it does not lead, in principle, to ionization of  $O_2$  (IE =  $12.07\,\mathrm{eV}$ ),  $N_2$  (IE =  $15.58\,\mathrm{eV}$ ),  $H_2O$  (IE =  $12.62\,\mathrm{eV}$ ),  $CH_3OH$  (IE =  $10.86\,\mathrm{eV}$ ), and  $CH_3CN$  (IE =  $12.26\,\mathrm{eV}$ ), typical G and S species present inside the source. The negative counterpart is that, by its use, the direct photoionization of organic compounds with IE >  $10\,\mathrm{eV}$  cannot be obtained and in these cases the use of a dopant (D) has been proposed. A suitable substance, added in relatively large amounts (with an IE value  $\leq 10\,\mathrm{eV}$ ), reasonably leads to the production of a large number of analyte ions through charge exchange (electron transfer) and/or proton transfer (Chapman, 1993). In the former case, the related mechanism can be described simply as:

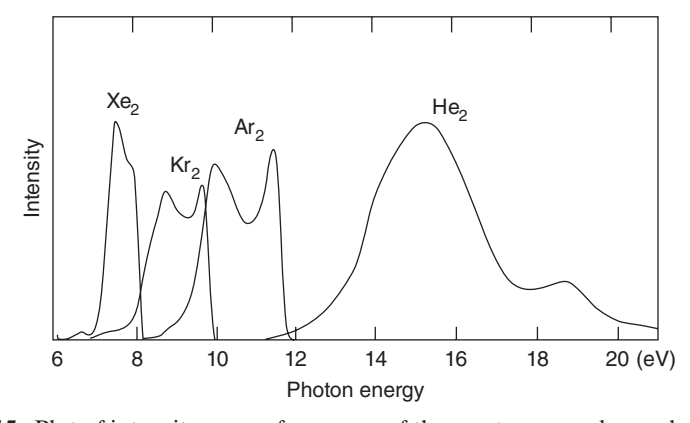


Figure 1.15. Plot of intensity versus frequency of the most commonly employed lamps.

$$D + hv \rightarrow D^{+}$$
  
 $D^{+} + ABC \rightarrow D + ABC^{+}$ 

and the internal energy of ABC+ can be calculated by

$$E_{\text{int}} = \text{RE}(D^{+\bullet}) - \text{IE}(ABC)$$

where RE (D<sup>++</sup>) is the recombination energy of the dopant ion and IE (ABC) is the ionization energy of the sample molecule. Relatively intense molecular ions are expected if RE(D<sup>++</sup>) is >IE(ABC). By considering that benzene and toluene, often used as dopants, exhibit RE values of ~9 eV (Einolf and Murson, 1972), the simple dopant mechanism described above seemed to be quite improbable.

Mainly two different instrumental configurations are employed for APPI experiments. The in-line geometry, due to Robb et al., has been derived from the standard heated nebulizer of the PE/Sciex 300 and 3000 (MDS Sciex, Concord, Ontario, Canada) series triple quadrupole mass spectrometers; in this case, the lamp is mounted perpendicular to the ion guide tube (Fig. 1.16). In the orthogonal geometry source, developed by Syagen Technology, starting from the scheme of the Agilent Technologies APCI source (Fig. 1.17), the heated nebulizer and the Kr lamp are, respectively, perpendicular and in-line with respect to the mass spectrometer ion path and there is no guide tube present.

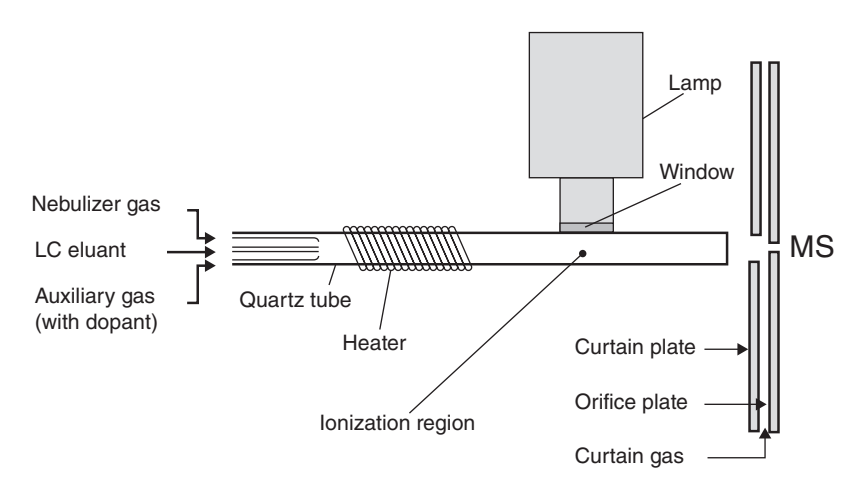


**Figure 1.16.** The APPI source with in-line geometry.

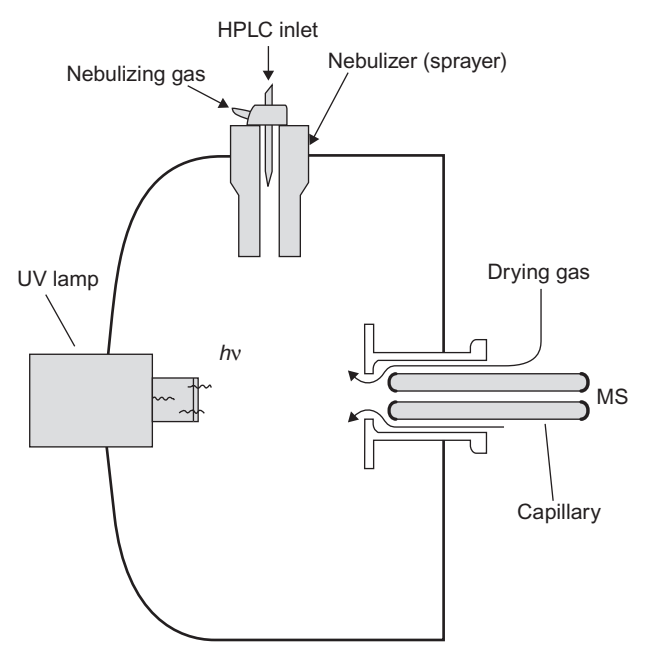


**Figure 1.17.** The APPI source with orthogonal geometry. (High-performance liquid chromatography = HPLC and UV = ultraviolet.)

#### 1.4 SURFACE-ACTIVATED CHEMICAL IONIZATION

Recently, surface-activated chemical ionization (SACI) has been proposed as an effective alternative approach to APCI and ESI in the MS analysis of biologically relevant molecules (Cristoni et al., 2005). A SACI experiment is particularly simple to realize. In a conventional APCI ion source, the corona discharge needle is substituted by a metallic surface and placed at a potential of a few hundred volts. The sample solution is vaporized in the usual way by the APCI nebulizer operating at a temperature in the range 350–400 °C. Even if, in principle, no ionizing conditions are present (i.e., electrons from the corona discharge are completely suppressed and the vaporizing conditions are far from those typical for the thermospray approach), the production of ionized molecular species (i.e.,  $[M+H]^+$ ,  $[M+Na]^+$ ,  $[M+K]^+$  ions) is observed in high yields.

In an investigation of the effect of several instrumental parameters on the efficiency of SACI, most attention was paid to the evaluation of vaporization parameters to test the hypothesis that ion evaporation can play an important role in the SACI mechanism. The data so obtained partially supported this hypothesis; by increasing the flow rates of either vaporizing gas  $(F_g)$  or solution  $(F_s)$  in the range 0.6–2.5 L/min and 10–150  $\mu$ L/min, respectively, a reasonably linear relationship of  $F_s$ /  $F_g$  versus ion intensity was obtained over a narrow range, after which saturation phenomena were observed. The positive role of the surface was proved by increasing its dimensions; in fact, a linear relationship between surface area and signal intensity was found by varying the former from 1 to  $4\,\mathrm{cm}^2$ .

After that investigation, a series of questions naturally arose that led to the need to understand the real role of the surface. Is it an active region for sample ionization, or does it simply behave as an electrostatic mirror leading to better focusing into the entrance capillary orifice of ions previously produced? If the latter hypothesis is true, how are the ions generated?

A reasonable ionizing mechanism might involve collisional phenomena occurring either in the high-density vapor or in the dilute gasphase region. The kinetic energy acquired by the molecules of the expanding gas could lead to effective collisional phenomena with the neutral species present inside the SACI source. The high density (atmospheric pressure) of the gas could lead to effective internal energy deposition through multicollisional phenomena, with the formation of ionic species, which in turn activate possible ion–molecule reactions. Alternatively, it could be hypothesized that protonated molecules are generated by collisionally induced decomposition of solvated analyte molecules through charge permutation and/or proton exchange processes.

The kinetic energies of the vaporized species were evaluated by simple calculations, performed on the basis of the experimental setup: They are in the 1–10-meV range, at least three order of magnitude less than those necessary to promote effective gas-phase collision-induced ionization and decomposition processes and, consequently, collisional phenomena cannot be held responsible for ion production.

Then, another aspect was considered, moving from the physical to a chemical phenomenon. At 20 °C, the dissociation constant for water  $(pK_w)$  is 14.1669, while it is 13.0171 at 60 °C and 12.4318 at 90 °C. Considering that

$$K_{\rm w} = [{\rm H}^+][{\rm OH}^-]$$

it follows that the  $[H^+]$  concentration changes from  $8.3 \times 10^{-8}$  to  $6.1 \times 10^{-7}$  M passing from 20 to 90 °C. In other words, the  $[H^+]$  concentration shows a clear increase with respect to temperature. These values are just related to pure water: The possible (and expected!) presence of

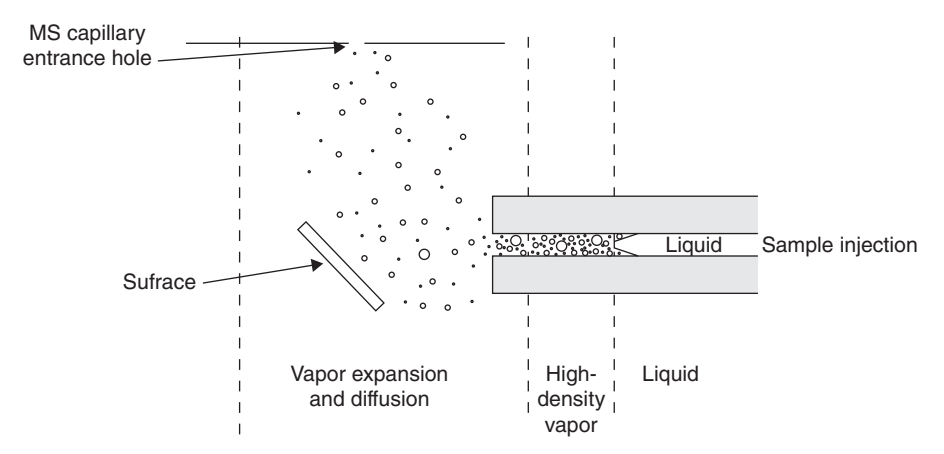


**Figure 1.18.** Scheme of a SACI ion source.

electrolytes even at low concentration would lead to a further increase of [H<sup>+</sup>] concentration. Consequently, it is more than reasonable to assume that during heating, but before solution vaporization, a decrease in pH of the solution takes place with the formation of protonated molecules from the analyte.

However, these considerations cannot explain the large increase in ion production (typically from  $10^4$  to  $10^6$  counts/s) observed when a metallic surface is mounted at  $45^{\circ}$ C with respect to the direction of vapor emission (Fig. 1.18). In the investigations of the SACI mechanism, it was shown that the best results are obtained not by holding the surface at ground potential, but by leaving it floating (i.e., insulated from ground). Interestingly, it was observed that in the latter condition the ionization efficiency increased with increasing nebulizing time; that is, the total elapsed time after nebulization was started. This result might be explained by considering that a number of ions, generated by the above described mechanisms, are deposited on the surface; by increasing the nebulizing time, this number increases to the point where a suitable potential is induced on the surface. The deposited ions then act as a protonating agent.

To investigate these ideas, a simple experiment based on the deposition on the metallic surface of a thin layer of deuterated glycerol was performed. Under this condition, when the analysis of the PHGGGWGQPHGGGWGQ peptide was performed by SACI, the signal of the  $[M + D^+]$  ion at m/z 1573 was observed to dominate (Fig. 1.19). This evidence is good for the participation of the chemicals present on the surface in the ionization phenomena occurring in SACI.

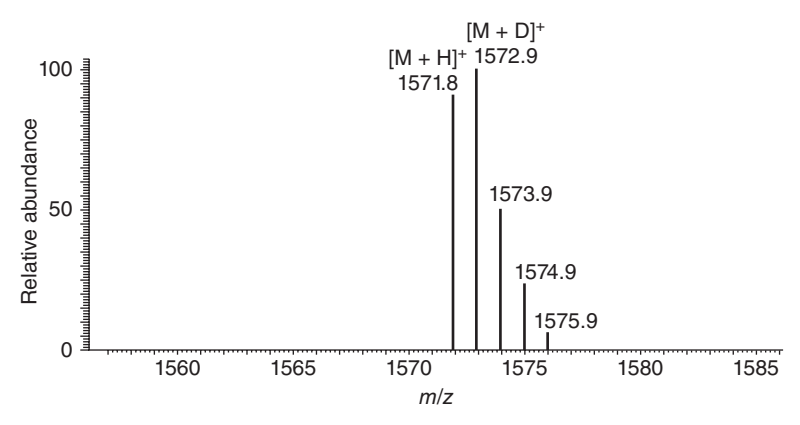


**Figure 1.19.** The SACI spectrum of the peptide PHGGGWGQPHGGGWGQ obtained by the pretreatment of the metallic surface with deuterated glycerol.

#### 1.5 MATRIX-ASSISTED LASER DESORPTION-IONIZATION

Matrix-assisted laser desorption-ionization (Karas et al., 1991) is based on the interaction of a laser beam [usually generated by an ultraviolet (UV) laser,  $\lambda = 337 \, \text{nm}$ ] with a crystal of a suitable matrix containing, at a very low level, the analyte of interest (usually the analyte/matrix molar ratio is on the order of 10<sup>-4</sup>). As depicted in Fig. 1.20, the laser beam-crystal interaction leads to the vaporization of a microvolume of the solid sample, with the formation of a cloud rapidly expanding in the space. The interaction gives rise to the formation of ionic species from the matrix (Ma), which exhibit an absorption band in correspondence to the laser wavelength, as Ma+ (odd electron molecular ions), Fr<sub>i</sub><sup>+</sup> (fragment ions), MaH<sup>+</sup> (protonated molecules), and Ma<sub>n</sub>H<sup>+</sup> (protonated matrix clusters). These species, through gasphase, ion-molecule reactions, gives rise to analyte positive ions (usually protonated molecules). Analogously, the formation of [M– H] anions from the matrix can lead to deprotonated molecules of analyte.

A detailed description of the MALDI mechanism is highly complex, due to the presence of many different phenomena:

- 1. First, the choice of the matrix is relevant to obtain effective and well-reproducible data.
- 2. The photon–phonon transformation, obtained when a photon interacts with a crystal and gives information on the vibrational levels of the crystal lattice, cannot be applied to the laser induced

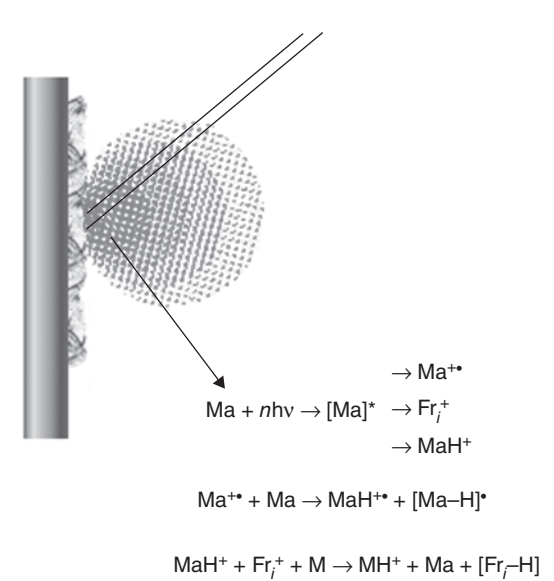


**Figure 1.20.** Interaction between laser beam and matrix (Ma) and analyte (M) solid samples, leading to the formation of protonated analyte molecules (MH<sup>+</sup>).

vaporization observed in MALDI experiments, due to the inhomogeneity of the solid sample.

- 3. The laser irradiance (laser power/cm²) is an important parameter: Different irradiance values lead to a vapor cloud of different density, and consequently the ion–molecule reactions can take place with highly different yields.
- 4. The solid-sample preparation is usually achieved by the deposition on a metallic surface of the solution of matrix and analyte with a concentration suitable to obtain the desired analyte/matrix ratio. The solution is left to dry under different conditions (simply at atmospheric pressure, reduced pressure, or under a nitrogen stream). This method is usually called the Dried Droplet Method. In all cases, what is observed is the formation of an inhomogeneous solid sample, due to the different crystallization rate of the matrix and analyte. Consequently, the 10<sup>-4</sup> molar ratio is only a theoretical datum: In the solid sample, different ratios will be found in different positions and the only way to overcome this is to average a high number of spectra corresponding to laser irradiation of different points.

To overcome this negative point, a new sample preparation method recently has been proposed (Molin et al., 2008). It is based on the

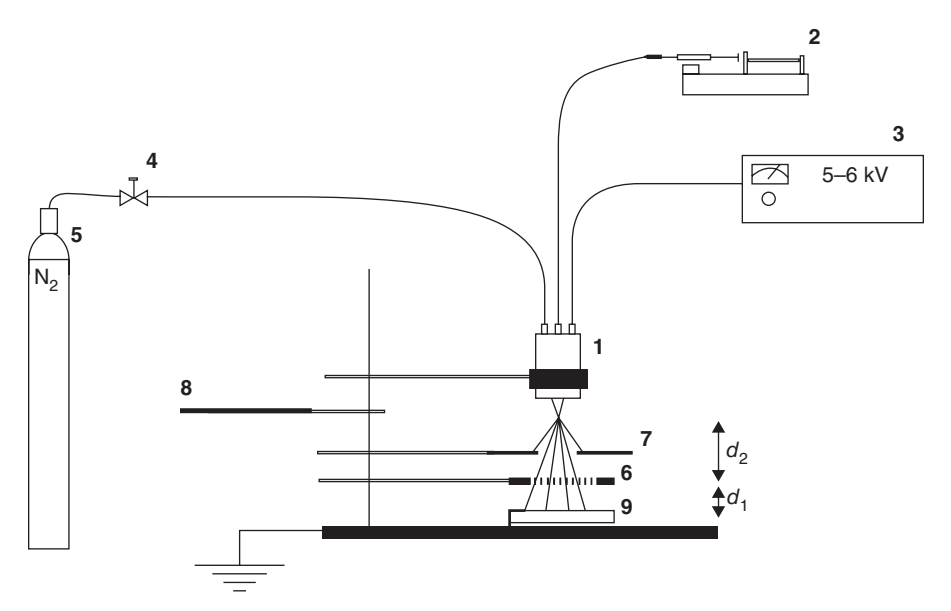


**Figure 1.21.** Schematic description of the sieve-based-device: **1** sprayer; **2** syringe pump; **3** DC power supply; **4** auxiliary gas flow regulator; **5**  $N_2$  cylinder; **6** sieve mounted on a stainless steel frame; **7** screen; **8** beam interceptor; **9** sample holder.

electrospraying of the matrix–analyte solution on the MALDI sample holder surface through a sieve ( $38\,\mu\text{m}$ , 450 mesh) (see Fig. 1.21). Under these conditions, a uniform but discrete sample deposition is obtained by the formation of microcrystals of the same dimension as the sieve holes.

With this approach:

- 1. Identical MALDI spectra are obtained by irradiation of different areas of the sample.
- 2. In the case of oligonucleotides, a clear increase of both sensitivity and resolution is achieved (see, i.e., Fig. 1.22).

The latter point can be explained in terms of the phenomena occurring by irradiation of a limited quantity of sample-matrix crystals. As the laser spot is elliptically shaped, with a maximum diameter of 100–150 µm, it follows that more than one sample-matrix crystal is irradiated and, considering the untreated sample holder (conductive glass) areas around the crystals, it may be hypothesized that the thermal energy associated with the laser beam is mostly deposited on the conductive glass surface, resulting in highly effective sample heating and

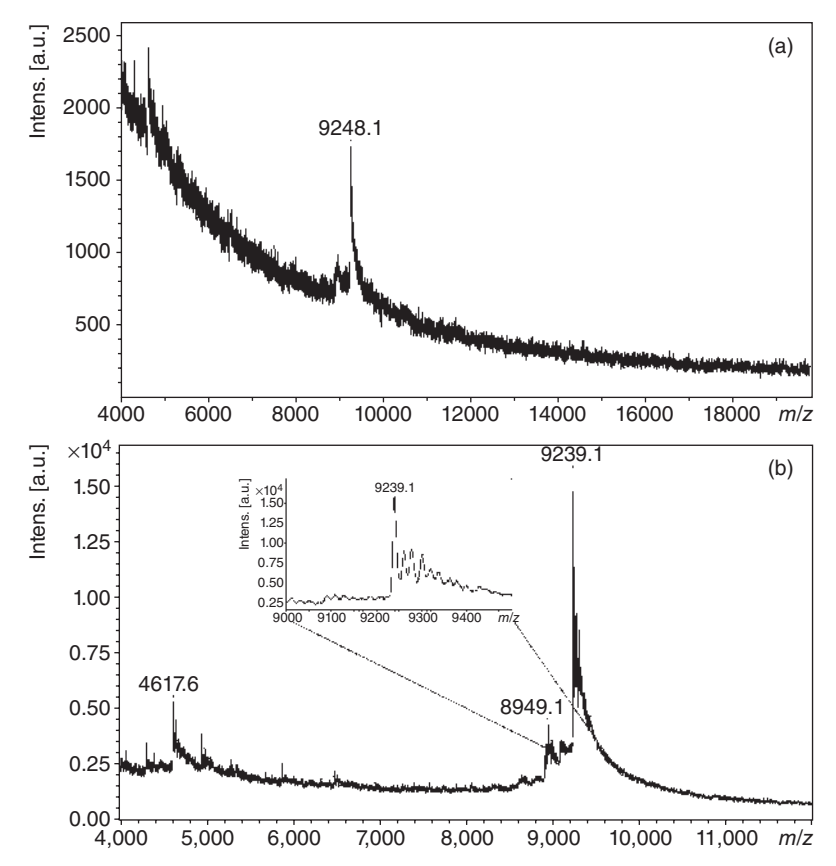


**Figure 1.22.** The MALDI-MS spectra of oligonucleotide obtained with traditional Dried Droplet deposition method (a) and obtained by spraying the matrix–analyte solution by a sieve-based device (b).

thus effective sample desorption. This result may explain the very high signal intensity achieved by this approach. In fact, irradiation of crystals obtained by the classical Dried Droplet method yields a signal intensity of 2000 arbitrary units (a.u.) that increases to 15,000 a.u. with SBD deposition (see Fig. 1.22).

The MALDI data originate from a series of physical phenomena and chemical interactions originating from the parameterization (matrix nature, analyte nature, matrix/analyte molar ratio, laser irradiation value, averaging of different single spectra), which must be kept under control as much as possible. However, the results obtained by MALDI are of great interest, due to its applicability in fields not covered by other ionization methods. Due to the pulsed nature of ionization

phenomena (an  $N_2$  laser operating with pulses of  $10^2$ ns and with a repetition rate of 5 MHz) the analyser usually employed to obtain the MALDI spectrum is the time-of-flight (TOF), which will be described in Section 2.4.

#### REFERENCES

- Agilent, technical literature (2007).
- Barber, M., Bordoli, R.S., Elliott, G.J., Sedgwick, R.D., and Tyler, A.N. (1982). Fast atom bombardment mass spectrometry, *Anal. Chem.*, **54**, 645–657 A.
- Beckey, H.D. (1975). Principles of Field Ionization and Field Desorption, *Mass Spectrometry*, Pergamon, London.
- Blades, A.T., Ikonomou, M.G., and Kebarle, P. (1991). Mechanism of electrospray mass spectrometry. Electrospray as an electrolysis cell, *Anal. Chem.*, **63**, 2109–2114.
- Bruins, A.P. (1991). Mass Spectrometry with ion sources operating at atmospheric pressure, *Mass Spectrom. Rev.*, **10**, 53–77.
- Cappiello, A. (2007). *Advances in LC-MS Instrumentation*, Elsevier, Amsterdam.
- Chapman, J. R. (1993). *Pratical Org Mass Spectrom*, 2nd ed., Wiley, Chichester, pp. 74–82.
- Chen, H.N., Genuit, W., Boerboom, A.J.H., and Los, J. (1983). Selective ion source for trace gas analysis, *Int. J. Mass Spectr. Ion Phys.*, **51**, 207.
- Cole, R.B. (2000). Some tenets pertaining to electrospray ionization mass spectrometry, *J. Mass Spectrom.*, **35**, 763–772.
- Cristoni, S., Rossi Bernardi, L., Guidugli, F., Tubaro, M., and Traldi, P. (2005). The role of different phenomena in surface-activate chemical ionization (SACI) performance, *J. Mass Spectrom.*, **40**, 1550–1557.
- De La Mora, J.F. and Locertales, I.G.J. (1994). The current emitted by highly conducting Taylor cones, *Fluid Mech.*, **260**, 155–184.
- Dole, M., Mack, L.L., Hines, R.L., Mobley, R.C., Ferguson, L.D., and Alice, M.B. (1968). Molecular beams of macroions, *J. Chem. Phys.*, **49**, 2240–2249.
- Einolf, N. and Murson, B. (1972). High pressure change exchange mass spectrometry, *Int. J. Mass Spectr. Ion Phys.*, **9**, 141–160.
- Favaro, S., Pandolfo, L., and Traldi, P. (1997). The behaviour of [Pt ( $\eta^3$ -allyl) XP ( $C_6H_5$ )<sub>3</sub>] complexes in electrospray ionization conditions compared with those achieved by other ionization methods, *Rapid Commun. Mass Spectrom.*, **11**, 1859–1866.
- Gatling, C.L. and Turecek, F. (1994). Acidity determination in droplets formed by electrospraying methanol–water solution, *Anal. Chem.*, **66**, 712–718.

- Gomez, A. and Tang, K. (1994). Charge and fission of droplets in electrostatic sprays, *Phys. Fluids*, **6**, 404.
- Harrison, A.G. (1983). Chemical Ionization Mass Spectrometry, CRC Press, Boca Raton.
- Karas, M., Bahr, U., and Gieβmann U. (1991). Matrix-Assisted Laser Desorpion Ionization Mass Spectrometry, *Mass Spectrom. Rev.*, **10**, 335–357.
- Kebarle, P. and Peschke, M. (2000). On the mechanisms by which the charged droplets produced by electrospray lead to gas phase ions, *Anal. Chim. Acta*, **11**, 406.
- March, R.E. and Todd J.F. (1995). Practical aspects of ion trap mass spectrometry VOL I,II,III CRC Press, Boca Raton.
- Mark, T.D. and Dunn, G.H. (Eds.) (1985). *Electron Impact Ionization*, Springer-Verlag, Wien.
- Molin, L., Cristoni, S., Crotti, S., Bernardi, L.R., Seraglia, R., and Traldi, P. (2008). Sieve-based device for MALDI sample preparation. I. Influence of sample deposition conditions in oligonucleotide analysis to achieve significant increases in both sensitivity and resolution. *J. Mass Spectrom.*, **43**, 1512–1520.
- Morrison, J.C. (1986). In J. H. Futtrell (Ed.), *Gaseous Ion Chemistry and Mass Spectrometry*., Wiley, New York, pp. 95–106.
- ORNL Review. (1995). *State of the laboratory*. Vol. **29** no. 1–2 http://www.ornl.gov/info/ornlreview/rev29-12/text/environ.htm
- Pfeifer, R.J. and Hendricks, C.D. (1968). Parametric studies of electrohydrodynamic spraying, *AIAA J*, **6**, 496–502.
- Rayleigh, L. (1882). On the equilibrium of liquid conducting masses charged with electricity, *Philos. Mag.*, **14**, 184–186.
- Revel'skii, I.A., Yashin, Y.S., Kurochkin, V.K., and Kostyanovshii, R.G. (1985). Pat. SU 1159412.
- Robb, D.B., Covery, T.R., and Briuns, A.P. (2000). Atmospheric Pressure Photoionization: an Ionization Method for Liquid Chromatography-Mass Spectrometry, *Anal. Chem.*, **72**, 3653–3659.
- Smith, J.N. (2000). Fundamental Studies of Droplet Evaporation and Discharge Dynamics in Electrospray Ionization, California Institute of Tecnology.
- Taylor, G. (1964a). Disintegration of water drops in an electric field, *Proc. R. Soc. London, Ser. A*, **280**, 283.
- Taylor, G. (1964b). Studies in electrohydrodynamics. I. The circulation produced in a drop by electrical field, *Proc. R. Soc. London, Ser. A*, **291**, 159–166.
- Thomson, B.A. and Iribarne, J.V.J. (1979). Field-induced ion evaporation from liquid surfaces at atmospheric pressure, *Chem. Phys.*, **71**, 4451–4463.

#### 44

- Wannier, G.H. (1953). The threshold law for single ionization at atoms or ions by electrons, *Phys. Rev.*, **90**, 817–825.
- Wigner, E.P. (1968). Symmetry principles in old and new physics, *Phys. Rev.*, **73**, 1002.
- Yamashita, M. and Fenn, J.B. (1984a). Electrospray ion source. Another variation on the free-jet theme, *J. Phys. Chem.*, **88**, 4451–4459.
- Yamashita, M. and Fenn, J.B. (1984b). Negative ion production with the electrospray ion source, *J. Phys. Chem.*, **88**, 4671–4675.
- Zelely, J. (1917). Instability of electrified liquid surfaces, *Phys. Rev.*, **10**, 1.